CALIFORNIA POLYTECHNIC UNIVERSITY SAN LUIS OBISPO

Scanning Electron Microscopy and Histology Imaging and Analysis of Decellularized Porcine Vessel

Advisor: Dr. Kristen O'Halloran Cardinal

Biomedical Engineering Department

Evans Moc, Jimmy Thai

6/9/2012

Abstract

This senior project analyzes the experimental units of Dr. Kristen Cardinal's research laboratory with decellularized and rinsed porcine vessels. Decellularized blood vessels provide possible alternatives to creating a blood vessel mimic (BVM) that can be used for the testing of intravascular devices. The vessels samples were prepared using dehydration, sectioning, and Hematoxylin & Eosin (H&E) staining protocols developed by Dr. Cardinal's research lab. After sample preparation, SEM imaging was conducted on the samples, and images of the tissue samples' fiber diameters and other architectural characteristics were analyzed using Image-J. Imaging of the samples prepared through H&E staining was conducted with the use of a wide field microscope under white light. These images were also analyzed with Image-J to evaluate for the presence of cells and measure the vessel wall thickness. Measurements of the vessels with Image-J show an average vessel wall thickness of 1.39 mm and 1.12 mm for the rinsed and decellularized vessels, respectively. Fiber diameters turned out to be 51.1 um and 42.4 um for the rinsed and decellularized vessels, respectively. T-tests were conducted on the data. The obtained p-values showed that there was no statistical difference between rinsed and decellularized vessels supporting the possible use of decellularized blood vessels for BVMs.

Table of Contents

List of Figures

List of Tables

Acknowledgements

We would first like to thank our advisors Dr. Kristen Cardinal and Aubrey Smith for the guidance they have given us. This project would not have been possible without the sponsorship of Dr. Kristen Cardinal. We would also like to thank Dr. Lily Laiho for her advising during the microscopy section of the project.

1. Introduction

1.1 Cardiovascular Disease and Treatments

Cardiovascular disease (CVD) accounts for the majority of deaths worldwide, with more than 17 million people dying from CVDs in 2008 alone. As seen in Figure 1, the primary cause of CVD deaths in both genders are ischaemic heart diseases, otherwise known as IHD, accounting for 46% of CVD deaths in males and 38% in females. IHD is a disease in which the myocardium receives a reduced blood supply due to a number of reasons, one of which being coronary heart disease (1). IHD usually presents itself as a pain in the chest following exertion, usually known as angina. This occurs due to the lack of oxyen-rich blood during the exertion period when the body requires more oxygen than normal. However, the underlying cause of the angina is usually heart disease, a serious pathology that may be fatal due to the complications that arise.

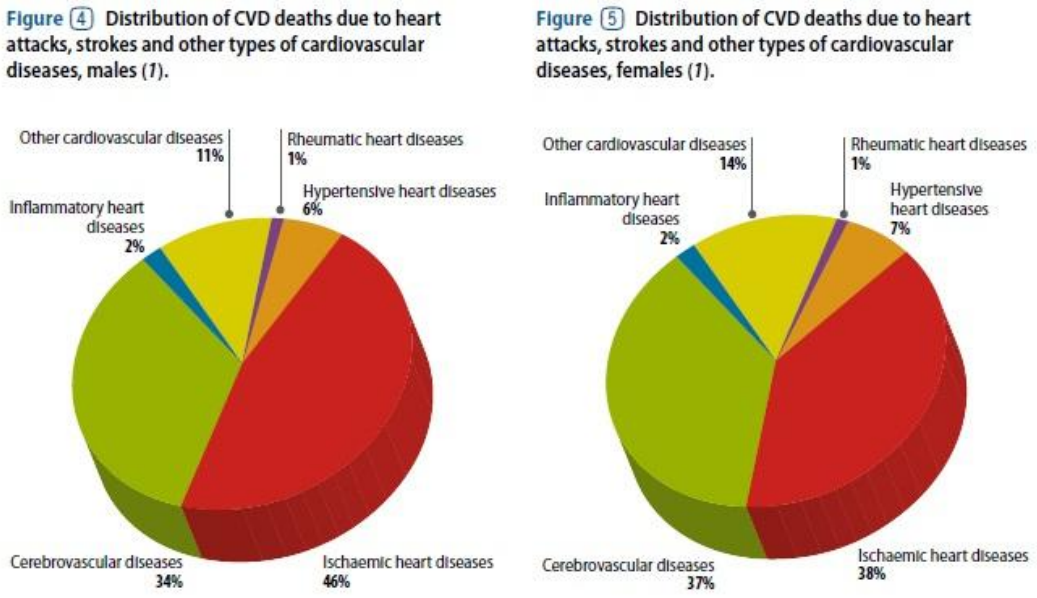

Figure 1. CVD Distribution. Distribution of CVD deaths due to various types of cardiovascular diseases. (1)

According to the Center for Disease Control and Prevention (CDC), the leading cause of death in the United States is heart disease, otherwise known as coronary heart disease (CHD) or coronary artery disease (CAD). CHD is a prominent disease within the United States, leading to an astounding 785,000 new cases of myocardial infarctions each year and another 470,000 secondary infarctions (2). The pathogenesis of this disease consists of the narrowing of coronary arteries due to atherosclerosis, or plaque buildup [Figure 2]. Plaque buildup may stem from a number of risk factors, the most common including smoking, obesity, diabetes, and hypertension (3). Once the plaque buildup occurs, the flow of oxygen to the heart becomes restricted which can cause angina or a myocardial infarction (4). The infarction, or heart attack, may lead to complications or prove fatal if left untreated.

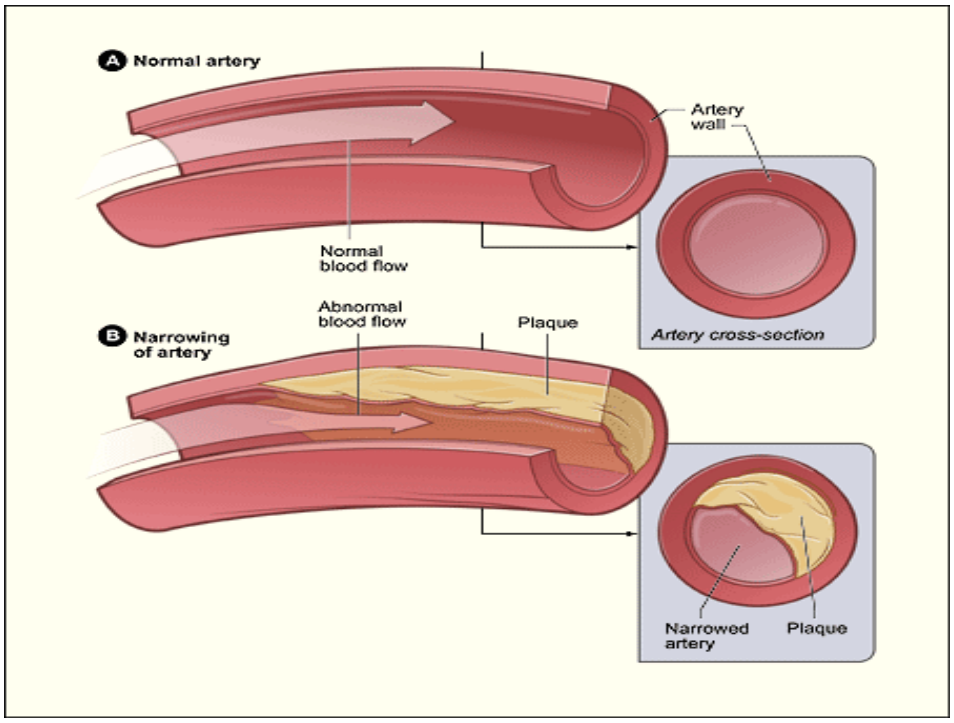

Figure 2. Atherosclerosis. A normal artery with no hindrance to blood flow compared to an atherosclerosis affected artery with a narrowed lumen. (3)

The prevalence of CHD in the United States and worldwide makes it a very costly disease. In 2010, the United States lost an estimated $316.4 billion due to aspects of treating heart disease, such as services and medications (2). As a result, the healthcare industry has a substantial amount of funding for finding safe and effective treatments for CHD.

Currently, treatments for CHD include various medications, such as ACE inhibitors and beta-blockers, to lower blood pressure in an attempt to lower the risk of myocardial infarction. ACE inhibitors prevent the muscles surrounding blood vessels from contracting, thus lowering the risk of high blood pressure and infarction by allowing normal or near-normal flow of blood to the heart (5). Beta-blockers block beta receptors, as their name implies; beta receptors are responsible for increasing heart rate among a number of other processes. By blocking these receptors, the patient's heart rate and risk of infarction decreases (6). While medication plays a major role in treatment, there are also surgical treatments available for patients, such as coronary artery bypass surgery. The surgery grafts arteries or veins from elsewhere in the body onto the coronary arteries to bypass the location of plaque buildup. This allows blood flow to circumvent the blockage and restores normal blood flow through an alternative pathway. However, this method possesses a large amount of risk due to the invasive nature of the surgery.

Another treatment for heart disease is the usage of stents [Figure 3], a mechanical tube placed within the coronary artery with the purpose of expanding the vessel to prevent reduced blood flow. The stent can be inserted and mounted at the specific location of the blockage using a balloon catheter, reducing the risk involved with the procedure (7). However, due to the foreign nature of stents, the body identifies the stent as a threat to the host and initiates an immune response in order to eliminate the threat. This immune response comes in the form of thrombus,

or clot, formation and cell proliferation at the site of the stent. The first type of stents made available to patients was bare-metal stents, those made entirely of metal with the sole purpose of mechanically widening the vessel. While these stents were effective in treating the blockage by opening the vessel, clot formation severely hindered their performance.

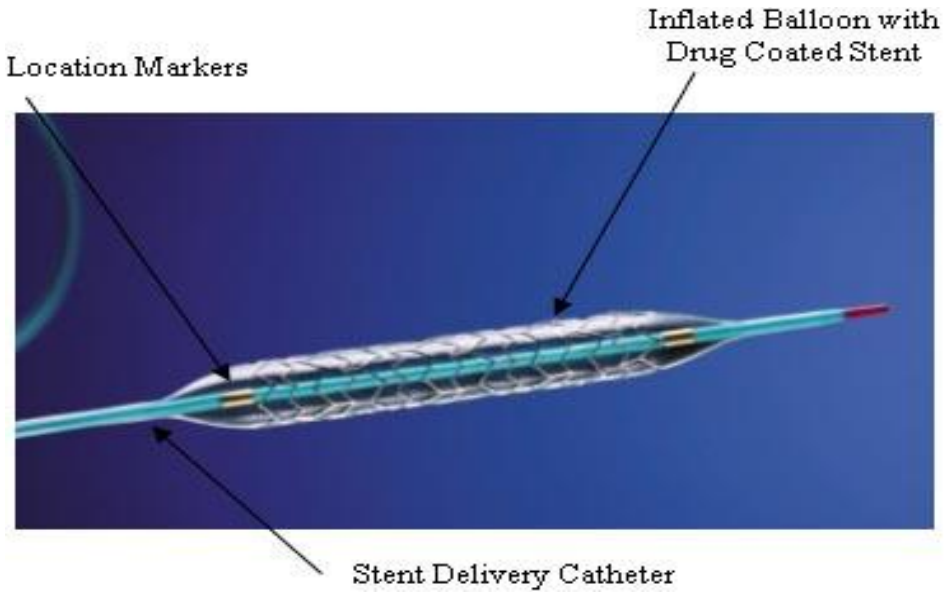

Figure 3. Stent. An example of a drug-eluting stent and its delivery method. (22)

As a result, modern stents tend to contain a drug in which it dissipates at the location of the blockage in an attempt to prevent cell proliferation and thrombus formation (7). The patient is also required to undergo antiplatelet therapy following the placement of a stent in order to hinder thrombus formation. However, there are new generations of these stents in development that will not require additional drugs or therapies. These new generations sents are biocompatible and absorbable, both of which should not run the risk of having platelet formation (8).

With these new generations of stents, extensive testing is required before they can successfully be marketed within the United States. A major component of testing involves placing it within bioreactors, called blood vessel mimics, similar to human blood vessels and

observing their efficacy within these vessels. These vessels, unfortunately, tend to be very expensive and time-consuming to manufacture consistently within specifications. As such, there is a high demand for a low-cost vessel that can be manufactured in a timely manner with consistent characteristics.

1.2 The Decellularized Blood Vessel Scaffold Model

Research of the decellularization of tissue has become large in the field of tissue engineering. This project involves the research of decellularized blood vessels - more specifically porcine carotid artery. The research currently being done by Professor Aubrey Smith supporting Dr. Kristen Cardinal's research laboratory investigates the effects of the decellularization of porcine carotid artery. The success of the research ultimately goes towards incorporating the decellularized vessel to be used as a graft to create a blood vessel mimic. Dr. Kristen Cardinal's research at Cal Poly involves using these blood vessel mimics as a model for the testing of intravascular devices (9). The use of blood vessel mimics in the testing of intravascular devices creates an intermediate to link the testing between in-vitro and in-vivo testing (9). As a result, intravascular devices can further be evaluated in a pseudo-physiological environment before in-vivo testing. With a greater understanding of an intravascular device upon the start of in-vivo testing, the cost of in-vivo tests may potentially be reduced as the number of animals tested is potentially reduced (9). The goal of the research is to determine if the effects of decellularization is consistent throughout all samples decellularized by the same method, which is perfusion decellularization (9). To assess the effects of decellularization, several properties of the blood vessel sample is tested. Important properties of a blood vessel scaffold that need to be evaluated include mechanical properties such as tensile strength and radial compliance, porosity, biocompatibility, and an ability to support an endothelium.

The mechanical properties of a scaffold are important in regard to tissue engineered blood vessels (TEBV). A radial compliance test of a blood vessel mimic (BVM) and the scaffold it is created on is currently one of the best ways to characterize the mechanical properties. The reason that compliance holds so much importance is because the compliance of a natural blood vessel is an integral property that helps serve the proper functioning of the vessel. Ideally, the scaffold that a BVM is created on should have the same compliance of a natural blood vessel (10). Compliance also influences several parameters such as flow and wall shear stress that regulate complex biological responses in terms of vascular remodeling (11). Researchers believe that increased shear stress caused by compliance mismatch is one of the main causes of intimal hyperplasia in blood vessel grafts (11).

Compliance plays a major role in the intravascular stent industry. To reiterate, the research done by this project will be incorporated to the testing of intravascular devices (9). BVMs need to imitate the properties of a natural blood vessel to accurately test the deployment of intravascular stents. Intravascular stents are designed to induce a certain amount of radial force to the vessel wall. BVMs that are too compliant will prevent the stent from operating ideally, and BVMs that are not compliant enough is likely to inhibit the proper deployment of the stent (9). In the presence of these factors, mechanical testing for radial compliance is crucial in regard to the development of a BVM to test intravascular devices.

Biocompatibility and the ability to support an endothelium are two other major properties that scaffolds must have. In the field of TEBV, biocompatibility testing serves to determine that the materials used in a scaffold are not harmful when interacting with cells (13). The ability to support an endothelium determines if endothelial cells are able to proliferate on the luminal surface of a blood vessel scaffold. Several factors are involved in endothelial proliferation.

Surface microstructure provides a large contribution in supporting cell adhesion (14). Mechanical properties of the scaffold also aids in the development of an endothelium. Research has shown that the growth rate of endothelial cells is directly related to the amount of shear stress experienced by the vessel wall (11).

The current designs of blood vessel scaffolds for use in TEBV attempt to meet the required parameters expected in an ideal artificial BVM. The result is an industry where much research has been devoted to creating scaffolds that utilize a variety of materials to accurately mimic a native blood vessel. The materials that have seen the most success are artificial and natural polymers.

1.3 Blood Vessel Scaffold Alternatives

1.3.1 Synthetic Alternatives

The gold standard in TEBV has been polytetraflouroethylene (ePTFE). It is currently being used in Dr. Cardinal's research as a scaffold for creating a blood vessel mimic (9). Outside of the field of TEBV, ePTFE has also been the gold standard of large vessel grafts for peripheral blood vessels (12). ePTFE is still being used as a large diameter (>6mm) vascular graft for vascular reconstructive surgery because of its success (12). ePTFE is a non-degradable polymer that has been shown through extensive research to be biocompatible (13). Additionally, the testing of the mechanical properties of ePTFE has displayed high burst pressure (13). Research has properly characterized the properties of ePTFE with the results being consistent and the ability to be reproduced (9). Aside from the mechanical properties and biocompatibility, ePTFE has been developed to have a microstructure for cells or other biological substances such as protiens to coat the luminal surface of the vascular graft (9, 14). The microstructure of the

surface can be changed depending on the composition of the polymer (9, 14). This allows manipulation of the desired microstructure to fit a certain application such as development of a vascular graft or even TEBV. By having a controlled microstructure on the surface of an ePTFE graft, an increase in cell interaction can possibly promote growth of an endothelium. Research is still currently being done to better characterize ePTFE, so improvements to its design can be made to overcome its disadvantages (will be discussed shortly) in the development of TEBV.

Poly(ethylene terphalates) (Dacron) has been used in similar applications to ePTFE (14). The most common use of Dacron is in the field of aortic replacement; however, it is also used in vascular graft applications less commonly (14). Research on the use of Dacron in replacement grafts has lead to the development of knitted designs to improve tissue integration with the graft (14). In the case of tissue engineering, this allows cells to better adhere to the surface of a knitted Dacron material. Tissue growth on Dacron provides is an advantage in terms of TEBV, but research shows that it can also be a disadvantage. Dacron grafts are designed to increase flexibility, elasticity, and kink resistance which are advantageous as a potential scaffold for TEBV; however, in the presence of tissue growth, the graft loses those properties that make the material advantageous (14). Even though there are apparent disadvantages to using Dacron in TEBV, it has still been effective in its current applications in aortic replacement. Ongoing research is still being done to develop Dacron to be used in TEBV.

Degradable polymers have also been studied for use as a scaffold for TEBV. One of the most popular degradable polymers used for blood vessel scaffolds is polyglycolic acid (PGA) (9, 14). Similar to the non-degradable alternatives, PGA can also be manufactured to with control of the microstructure (9). The ability of PGA to degrade has been a driving force for the development in its use for tissue engineering (14). The mechanism for the degradation of PGA

has been carefully characterized, and due to the biocompatibility of the process, PGA has been desirable in its application in tissue engineering (14). Drawbacks exist for the use of PGA in tissue engineered vascular grafts; however, research is still being done to design a PGA graft that overcomes the drawbacks.

The advantages of each synthetic alternative would make one believe that these choices are optimal for use in TEBV; however, the synthetic alternatives also have disadvantages that have a significant effect in its application in TEBV. A major disadvantage of the synthetic alternatives is the mismatch of compliance when compared to native blood vessels (14). As stated previously, mismatches in compliance has major effects on cell proliferation and wall shear stress. This makes development of an endothelium difficult even with the aid of the surface microstructure. The use of synthetic scaffolds creates a BVM that is physically dissimilar to a native blood vessel (11). Figure I shows a visual comparison of a native porcine carotid artery to BVM constructs using poly(glycerol sebacate) (PGS) and PLGA scaffolds.

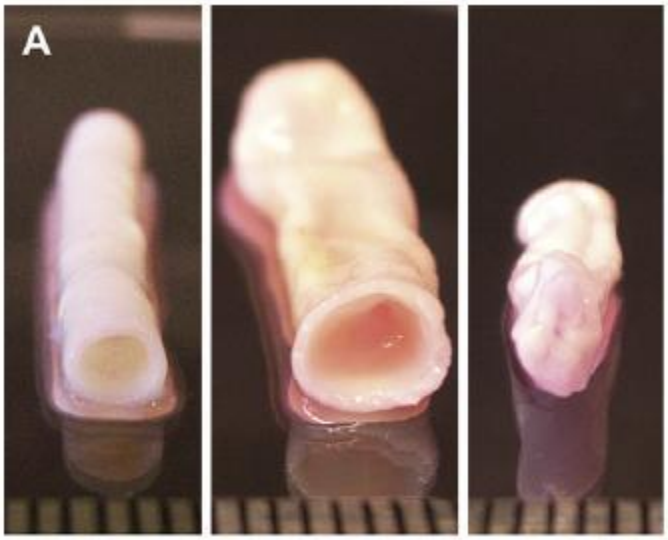

Figure 4. A comparison of a native porcine carotid artery, PGS constructed BVM, and PLGA constructed BVM (shown from left to right) (11).

The synthetic alternatives have only been consistently successful in large diameter vessel applications (12). When used in small vessel applications, the synthetic alternatives tend to have problems associated with clot formation (12, 13). Another disadvantage is the absence of a layer similar to adventitia seen in native blood vessels which is a important component to a blood vessel's physiology (9). Research has been done to mitigate these disadvantages. A.P. Zhu et al. investigated the effects of chitosan/heparin modified surface of ePTFE as an attempt to determine the feasibility of reducing thrombus formation in small diameter grafts (12). The limitations of synthetic grafts have led to the development of biological alternatives.

1.3.2 Biological Alternatives

A biologic scaffold composed of collagen has been in the process of research and development since 1986 which at the time, Weinberg and Bell researched into developing a scaffold that had a primary composition of biologic components (15). The primary components of the scaffold were bovine aortic endothelial cells, smooth muscle cells, and adventitial fibroblasts (15). To imitate the different layers of tissue seen in natural blood vessels, they molded culture medium, collagen, and smooth muscle cells around a mandrel to make a tubular middle layer representing the media of an artery (15). For mechanical support, the scaffold needed a layer of Dacron that was made into a mesh sleeve and slipped over the middle layer of the scaffold (15). The adventitial fibroblast was then cast over the Dacron layer to produce the most outer layer representing the adventitia layer of a blood vessel (15). This scaffold design was removed from the mandrel and was tested for mechanical strength (15). The researchers also attempted to line the luminal surface of the scaffold with endothelial cells to create the most inner layer (15). The resulting mechanical test determined that the scaffold had similar

characteristics of the mammalian muscular artery (15). The model created by Weinberg and Bell has been studied further by other researchers because it was one of the first scaffolds that represented the physiological characteristics of a native blood vessel.

L'Heureux et al. were researchers that decided to use and expand on the scaffold model that Weinberg and Bell developed (13). The researchers wanted to create a scaffold that was entirely supported by substances created by cultured human cells (13). The media layer of the scaffold consisted of a sheet of human vascular smooth muscle cells wrapped around in a tubular form (13). The media layer was then wrapped around by a sheet of human fibroblast to produce an adventitia layer (13). Endothelial cells were then seeded on the luminal surface of the scaffold to produce a three layer BVM with a similar physiology of a native blood vessel (13). The BVM created by L'Heureux et al. became the first TEBV to be composed of biologic materials (13). Mechanical testing of the BVM showed that burst pressures were high but within an acceptable range (13). The problem with their BVM was a low compliance when compared to the human saphenous vein, but it was shown to have a higher compliance than ePTFE vascular grafts (13). Figure II contains an image of the BVM developed by L'Heureux et al.

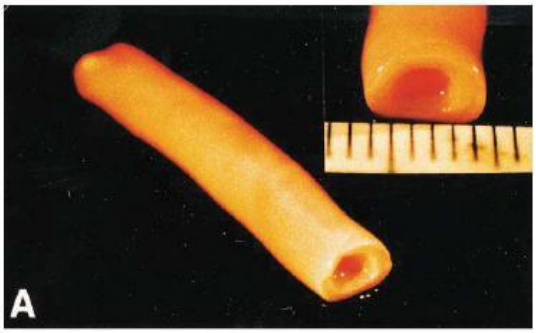

Figure 5. Blood vessel designed from biological components. The vessel is created from human smooth muscle cells, human fibroblasts, and endothelial cells (13).

The limitations of the biologically created scaffold has further led to research on using decellularized tissue to produce a biological scaffold composed of an extracellular matrix.

1.3.3 Decellularized Scaffold

Another method of obtaining a biologic scaffold is through the process of decellularization. Decellularization of tissue has recently become a growing a field of research in tissue engineering. Decellularized tissue have been used in a variety of applications such as pre-clinical animal studies and human clinical studies (16). The advantage of using decellularized tissue is that it is even tolerable in a xenogeneic host. The body normally activates the foreign body and inflammatory response as a result of a foreign body reaction to the cellular antigens when a graft of xenogeneic origin is implanted (16). The ECM of tissue is usually compatible throughout most species which makes implantation of decellularized tissue as grafts more successful in terms of the avoidance of a foreign body response (16). Decellularized xenogeneic tissue have been used in the development of heart valves. Schenke-Layland et al studied the mechanical properties and the recellularization of the decellularizaed xenogenic tissue for use in heart valve replacement (17). A decellularized scaffold must be fully decellularized to avoid immune responses post-implantation, and the scaffold must be able to be efficiently seeded with cells (17). In the field of TEBV, a study done by Conklin et al evaluated the success of a decellularized vascular xenograft coated with heparin for the use in small diameter vascular grafts (18). The study found that the decellularized vessels were similar in compliance and able to host a population of smooth muscle cells on the vessel wall (18). These studies have led to further development of BVM using decellularized vessels as scaffolds; however, the consistency of the mechanical properties as well as the success of decellularization have yet to be verified. The purpose of the research done by Professor Aubrey Smith is to verify that changes in the

mechanical property and surface morphology are consistent in all samples decellularized by the same process.

1.4 Purpose: Analysis of Consistency of Decellularization

This senior project is based off the the research that is done by Professor Aubrey Smith. This project is sponsored by Dr. Kristen Cardinal for the purpose of testing the effects of the decellularization process on a porcine carotid artery. The research is part of the overall goal of Dr. Kristen Cardinal's research laboratory in creating a BVM that has the same characteristics as a native blood vessel to be used in the testing of intravascular devices (9). Decellularized blood vessels are promising substitutes as they do not exhibit the same limitations of PTFE and PGA in terms of compliance. This senior project involves the use of the scanning electron microscope (SEM) and histology to analyze the morphology and confirm the success of decellularization respectively.

The decellularization process changes the surface morphology of the blood vessel being decellularized. The purpose of the SEM segment of this senior project is to image (using the SEM), measure, and statistically analyze surface features such as fiber width to determine whether it remains the same for all decellularized samples. The purpose of the histology segment of this senior project is to confirm the success of the decellularization process in all samples. The histology images will also be used to measure vessel wall thickness for statistical analysis to determine the significance of change in thickness.

The results obtained in this senior project will support the research done by Professor Aubrey Smith and ultimately Dr. Kristen Cardinal's research laboratory in search of a successful BVM that would provide the most accurate and reliable model to test intravascular devices.. This

senior project is significant towards the development of a BVM that accurately mimics the properties of a native blood vessel; the significance will extend into the field of intravascular devices because the creation of a BVM with native blood vessel properties will aid in the testing and development of intravascular devices.

2. Methods

2.1 SEM Analysis

2.1.1 Introduction to the SEM analysis

The SEM utilizes a beam of electrons by passing it through the sample in a raster pattern in order to image the surface of the sample, providing information about the sample such as topography, composition, and directionality. Usually, the beam of electrons is created by the passing of current through a tungsten filament in order to boil off electrons from the tungsten. The electrons are then accelerated and passed through an objective to focus into a beam with a diameter within the nanometer scale. When the beam hits the surface of the sample, electrons are ejected from the sample surface and collected by an analyzer. A driver translates the number of electrons counted and produces the image of the sample surface on the computer screen. However, in order for the sample to be image, the user must place the sample inside a chamber with a vacuum inside. As a result, the sample must be free of any moisture or foreign particles that may depart from the sample and cause damage to the microscope. This is accomplished through the use of dehydration protocols which effectively sterilize and rid the moisture from the sample.

2.1.2 Methods of Fixation and Dehydration

There are various protocols to choose from for dehydration of samples for use with the SEM. However, because this project uses biological tissue samples, the dehydration protocol must be tailored to effectively dehydrate the samples. Thus, the choices then become limited to a handful rather than a diverse set. One of these protocols, retrieved from the University of Alabama (UA), effectively defines a general schedule for preparing animal tissue for SEM

imaging; for comparison purposes, their general protocol is given in Appendix D (21). In their protocol, it calls for 2.5% glutaraldehyde for primary fixation and 1-4% osmium tetroxide in distilled water for secondary fixation. Dehydration of tissue samples using a series of alcohols is a relatively harsh method which can change structures to the proteins within the sample. Tissue fixation effectively halts protein processes so the surface micro-structure and bulk is unaffected by the dehydration process. Doing so would produce results that accurately represent the effects caused by the decellularization and rinsing processes rather than the effects of the dehydration process.

There are several methods of tissue fixation. For tissue analysis under a SEM, chemical fixation is most often the best option. In literature, due to its rapid and irreversible effects, glutaraldehyde is used as a tissue fixative for SEM more often than formaldehyde (19). Glutaraldehyde is a crosslinking fixative which acts by linking proteins together through the creation of covalent bonds. Soluble proteins that may be otherwise denatured or rinsed from the tissue due to the dehydration process are irreversibly linked to the cytoskeleton of the cell (19). The result is a tissue with its morphology preserved even after the dehydration process.

Osmium tetroxide is used as the secondary fixative in the protocol. Osmium tetroxide acts as a fixative for lipids as glutaraldehyde does for proteins. It reacts with the heads of lipids to crosslink them with the proteins in a glutaraldehyde fixed sample (20). Classed as an oxidizing agent, osmium tetroxide denatures proteins if used alone. Since glutaraldehyde is used first, the effect of osmium tetroxide on protein is essentially mitigated.

The actual dehydration process is done by submerging the tissue sample into different concentrations of alcohol in series from low to high. Nearing the end of this process the sample

loses moisture content and shrinks. The removal of all moisture content allows the tissue sample to be effectively imaged under the SEM.

2.1.3 The Dehydration Protocol

For the Scanning Electron Microscope portion of this project, the dehydration protocol, developed in Dr. Kristen Cardinal's lab and used in Professor Aubrey Smith's thesis, was applied for her tissue samples that was used to dehydrate the sample for SEM imaging. The specific dehydration process consisted of eleven steps which are listed in Appendix A. The protocol differs from the UA protocol in that it did not require a secondary fixation, mounting of the specimen with graphite, nor coating of the specimen. Since only fiber diameter was being studied through the SEM analysis, secondary fixation of the vessels was not needed. Surface morphology of the vessel's lumen at the micrometer scale was more largely affected by the protein matrix. The mounting of the specimen on graphite is usually needed for SEMs that utilizes higher energy electron beams; in this project, a table top SEM was used and the accumulation of charge did not become a problem for imaging, so a graphite sheet was not needed to mount the specimen on. Since resolution was acceptable at the low magnifications used, there was no need to gold sputter the specimen to improve image quality.

2.1.4 SEM Imaging

A Scanning Electron Microscope (SEM) was used, specifically the Hitachi Tabletop Microscope model TM-1000, to image the lumen of the decellularized and rinsed porcine vessel samples acquired in Professor Aubrey Smith's research. After dehydration, the vessel specimen was fixed to the SEM sample stage using double sided tape. The height of the sample stage

needed to be adjusted with sample preparation tool before placement of the vessel specimen and stage into the SEM. Proper height adjustment was important to make sure the stage and sample cleared the ceiling of the sample feed and was high enough for the SEM to bring an image of the vessel surface into focus. Several sets of images were taken of each sample at the scales of 20, 50, and 200 um.

2.1.5 Image Analysis

ImageJ, an open-source imaging software, was used to analyze the images taken with the SEM. This software allows for analysis and comparison of the fiber diameters and node distance of each tissue sample. An image from each vessel specimen was opened with Image-J for measurement analysis. The primary purpose of imaging the vessel lumen using SEM was to measure for fiber diameter and node distance.

Image-J allows the user to take measurements in an image using their line tool. After using the line tool, Image-J outputs the measurement in units of pixels. Because pixel is not a commonly used unit to measure lengths in biologics, conversion from pixels to micrometers was necessary. This is easily achieved using a conversion tool in the Image-J program. The conversion tool requires the user to input a known length (micrometer) of a ruler in the given image and the length in pixels of the same ruler. Measurements taken after that using the line tool will output lengths with the units of micrometers. Detailed instructions on how to measure lengths in Image-J is given in Appendix E.

To obtain an accurate measure of fiber diameter for the images of each sample, four line measurements were taken of four different fibers. The lengths of the four lines were averaged to obtain a “true” value of the fiber diameter. Since the image analysis required the user to make

measurements, the success of this project depended on the quality and consistency of the images retrieved and analyzed from the SEM.

Node distances were measured by taking the distance between two fibers. Four measurements of the node distances were taken of each image and averaged to obtain a “true” value, similar to the method used for obtaining fiber diameters.

Sixteen SEM images were used for analysis of fiber diameters and node distances, eight samples from the rinsed group and eight from the decellularized group. The true values for all sixteen images were calculated and compared to each other using statistical analysis for any significant differences.

2.2 Histology

2.2.1 Introduction to Histology

Histology is the study of the microscopic features and characteristics of biological materials, such as plants and animals. This process provides information regarding the morphology, architecture, and composition of tissue. The process consists of a number of steps, beginning with fixation. Fixation allows preservation of the shape and sizes of the cells present on the tissue by immersing the sample into a chemical that cross-links proteins, typically formaldehyde or gluteraldehyde. Next, processing occurs to remove any trace amounts of moisture in the sample. This step prepares the sample for paraffin wax, relevant in the subsequent step, which does not mix with water. The sample is then embedded into paraffin wax to allow for sectioning to occur easily. Sectioning involves cutting thin slices of the embedded sample and placing these slices on to glass slides. The mounted samples are stained to produce color specific features within a tissue sample, highlighting various characteristics such as cell presence, nuclei, and any notable identifiers. Different staining methods exist depending on the feature that is desired to be highlighted. For this project, hematoxilyn and eosin staining will be used to highlight the nuclei and collagen matrix respectively.

2.2.2 Sectioning

Sample blocks for sectioning were provided to us through Professor Aubrey Smith's research sponsored by Dr. Kristen Cardinal. Each block had a specimen sample of either a decellularized or rinsed vessel embedded into the paraffin wax block. Sectioning of the block produced cross sections of the vessel for staining, imaging, and analysis. The thickness of each section is important for analysis. A section cut too thick prevents light from penetrating the

sample during optical microscopy, and a section cut too thin will produce sections that do not contain the entirety of the cells being analyzed. Each section was cut 7 micrometers in thickness which is the standard thickness for analyzing sections of the porcine vessel. To assure for accurate analysis during the optical microscopy, two slides containing two sections each were obtained for every sample block number. The two slides were separated into groups A and B and stained separately. This provided us with a backup slide in case some sections were unacceptable for imaging or an error happened during the staining process for one group of slides.

2.2.3 H&E Staining

For the scope of this project, the protocol for staining tissue samples will be taken from Dr. Kristen Cardinal's Biomaterials course. An overview of the process and corresponding H&E protocol is outlined in Appendix B and C, respectively.

The notable chemicals in the staining process are: xylene, hematoxylin, and eosin. The purpose of xylene during the staining process is for the removal of the paraffin wax in each slide containing a section of the vessel. Xylene is a hazardous chemical and was only handled in the fume hood. Hematoxylin is a chemical used to highlight any nuclei present in each tissue section. Nuclei in a tissue section are stained purple when exposed to hematoxylin. Eosin is a chemical used to highlight proteins which includes the ECM. Proteins and ECM are stained pink when exposed to Eosin. While the other chemicals in the staining protocol are of equal importance in providing the best results of an H&E stain, hematoxylin and eosin are the chemicals that provide the ability to identify nuclei and the protein matrix present in each tissue sample, and xylene removes the unwanted residue of paraffin wax from each section for proper slide imaging.

2.2.4 Wide Field Optical Microscope Imaging

An Olympus Wide-Field Microscope was used for this project to image histology slides at magnifications of 4X, 10X, and 40X. This microscope has a digital output to a corresponding computer where a live preview of the slide at the appropriate magnification could be observed. Before each usage, the life of the fluorescence bulb was documented into a notebook nearby the microscope.

Preparation of the slides consisted of removing the slides from the slide box and placing them onto an adjustable height platform. The microscope was turned on through a series of steps and then calibrated through the live preview on the computer. First, the main power supply for the microscope and a separate power switch for the digital camera were turned on. Then, the lenses were switched to FW2 and a number greater than 5 chosen to avoid a filter. Finally, a pin near the camera was extruded from the microscope to physically allow digital image viewing of the sample on the computer rather than through the eye piece. Following these steps, the calibration process began using the image on-screen.

Calibration consisted of adjusting the height of the platform until a visible image of the sample was obtained. Once a rough view of the sample appeared, the option to "Auto-Calibrate White Balance" was selected. This auto-corrected the background color to clearly show the sample in question. A knob for fine focus allowed for elimination of any blur still existing on the image following these steps. Additionally, if the image was too dark, a knob at the base of the platform adjusted the intensity of the light beneath the sample.

2.2.5 Image Analysis

Images taken with the Wide-Field microscope were analyzed in Image-J to identify cell presence and estimate thickness of the lumen wall. Image-J provides measurements in the unit of pixels, so a method to convert pixels to a common scale which was millimeters for this project was required. SEM image analysis using Image-J used the calibration tool provided by Image-J. However, the images obtained with the wide field microscope was provided with a magnification, but without a scale, so the calibration tool could not be used. An alternative method was used where a ruler was imaged at a magnification of 4X. Professor Aubrey Smith provided the image of the ruler at a magnification of 4X, and is shown in Figure 6. One side of the ruler (one side of one of four squares) was known to be 1 mm in length. The side was then measured in Image-J to obtain its length in the units of pixels. With the known distance and the measured distance, a conversion factor was obtained by taking the ratio of the known distance in millimeters to the measured distance in pixels. The following equation was the ratio used.

$$Conversion\ Factor = \frac{Known\ Length\,(mm)}{Measured\ Length\,(pixels)}$$

The conversion factor was calculated to be 0.003205, and was multiplied to all the Image-J measured values with the units of pixels.

All decellularized, rinsed, and control (fresh and unprocessed) vessels were measured for wall thickness. Careful attention was needed because measuring to a consistent radius of curvature was important to obtaining accurate measurements. After measuring all the vessels at 4X magnification, the measurements were all multiplied to the conversion factor to convert the units from pixels to millimeters. The measurements were subsequently analyzed using statistical methods.

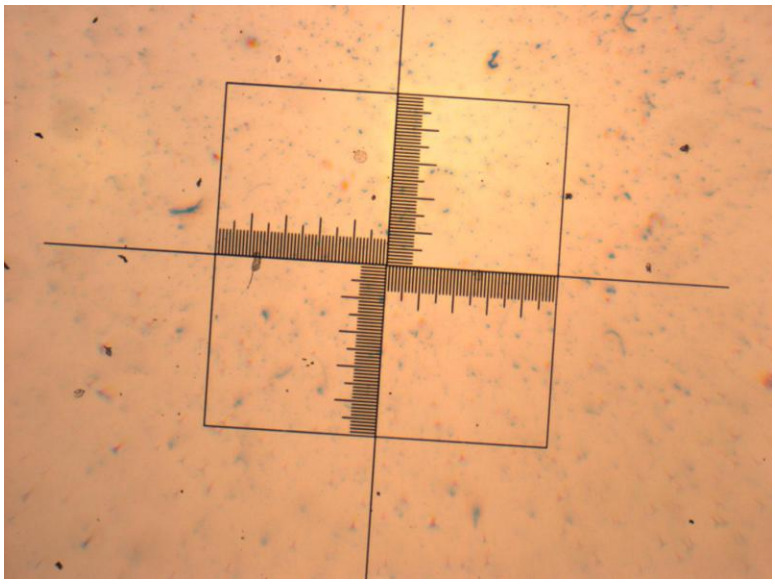

Figure 6. Image of the ruler. One side of a square is known to be 1mm.

Four measurements were taken of each sample and averaged in order to provide an accurate estimate of the wall thickness of each sample.

Additional image analysis was also done by looking for the presence of cells. For this analysis, Image-J was not needed, and a 10X or 100X image was only needed to qualitatively determine if cells were present in the image. This was conducted by simply looking for successful hematoxylin stains of nuclei which show up as blue dots on images of vessels containing nuclei. If the blue dots are present, the vessel was documented to contain cells.

2.3 Statistical Analysis of Results

The measurements for both H&E and SEM samples were analyzed through a comparison between rinsed and decellularized samples. A two-tailed Student's T-Test for two samples with unknwon variances was carried out on the data in Microsoft Excel using the Data Analysis tool. For this analysis, the null hyporthesis was that there is no difference between the mean data of

both groups, rinsed and decellularized, while the alternative hypothesis is that there is a difference between the two groups. The T-test had a critical value of 0.05, meaning any p-value below 0.05 would represent a rejection of the null hypothesis and claim a significant difference between the average true values of that certain attribute with a 95% confidence.

2.4 Materials List

The following is a list of the materials required to complete this project. All materials will be provided by Professor Aubrey Smith and Dr. Kristen Cardinal. The SEM and Wide-Field Fluorescent microscope will be provided by Cal Poly's Biomedical Engineering Department.

1. Porcine Vessels
2. Ethanol at various concentrations
3. Xylene
4. Hematoxlin
5. Distilled Water
6. Clearifier
7. Bluing agent
8. Eosin

3. Results

3.1 Analysis of SEM Images

The fiber diameter (width) was measured in the SEM images of both the decellularized and rinsed vessel samples. A qualitative analysis of the images revealed that the lumen of each vessel exhibited some patterns within its surface morphology; tissue fibers in each image had common directionality and consistent fiber diameters.

Measuring fiber diameter was important to compare differences in morphology between a decellularized versus rinsed sample. Table 2 contains data from the Image-J analysis of the fiber diameters of rinsed vessels, a representative SEM image of rinsed vessels is shown in Figure 7. In Table 3, data from the Image-J analysis of the fiber diameters of decellularized vessels is tabulated. A representative of decellularized vessels is shown in Figure 8. Sample 6R and 6D were omitted from analysis due to fibers being indistinguishable on Sample 6R, resulting in removal of 6D to maintain two samples of the same sizes.

The following are SEM fibers of a rinsed vessel at the various magnifications taken, showing details of the surface of the lumen at three different magnifications. Fibers of the collagen can be seen in the first image at 200 microns.

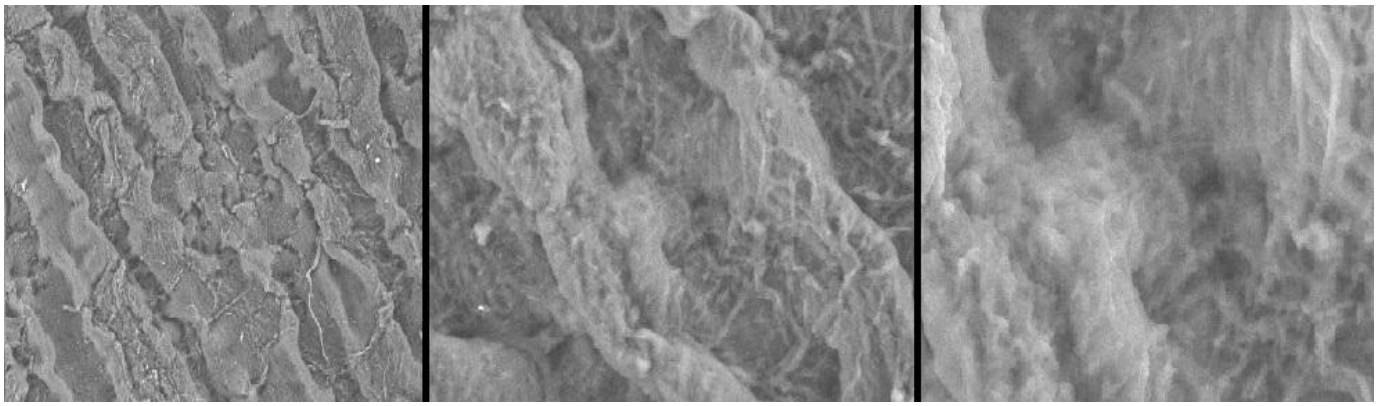

Figure 7. Rinsed Vessel SEM. An SEM micrograph of a rinsed vessel at 200, 50, and 20 microns (left to right). Sample 3R.

The following are SEM fibers of a decellularized vessel at the various magnifications taken, showing details of the surface of the lumen at three different magnifications. Fibers of the collagen can be seen in the first image at 200 microns.

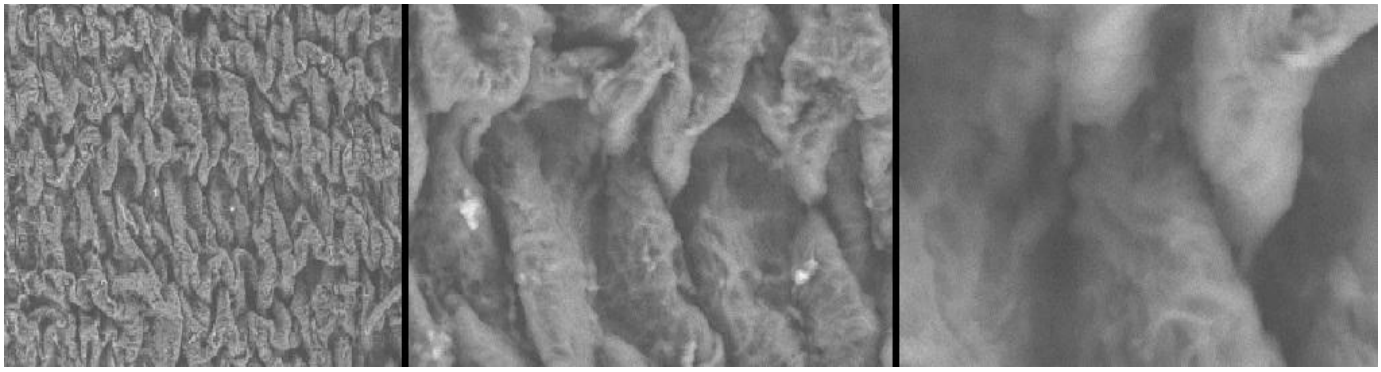

Figure 8. Decellularized Vessel SEM. An SEM micrograph of a decellularized vessel at 200, 50, and 20 microns (left to right). Sample 8D.

The average fiber diameters were put into graph form shown in Figure 9 with standard deviation bars to effectively show the difference between rinsed and decellularized fibers in SEM analysis.

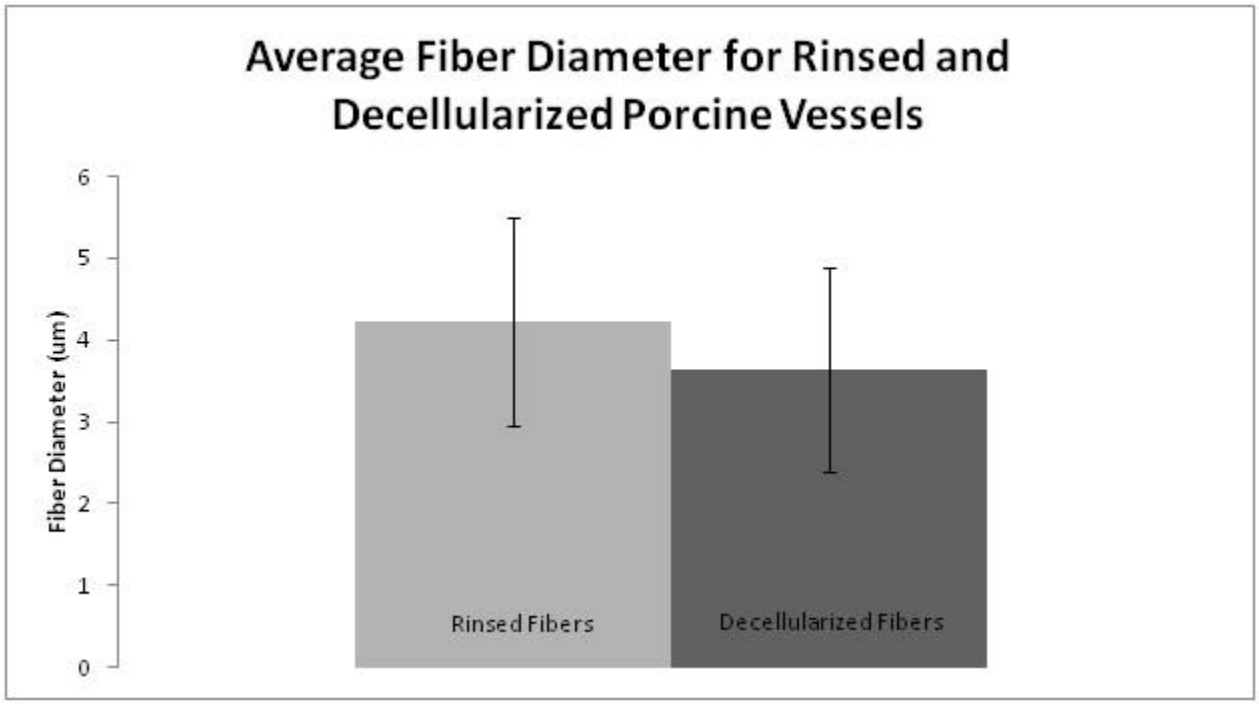

Figure 9. Graph of Fiber Diameters. The average fiber diameters of rinsed and decellularized vessels are shown.

The average node distances were put into graph form shown in Figure 10 with standard deviation bars to effectively show the difference between rinsed and decellularized fibers in SEM analysis.

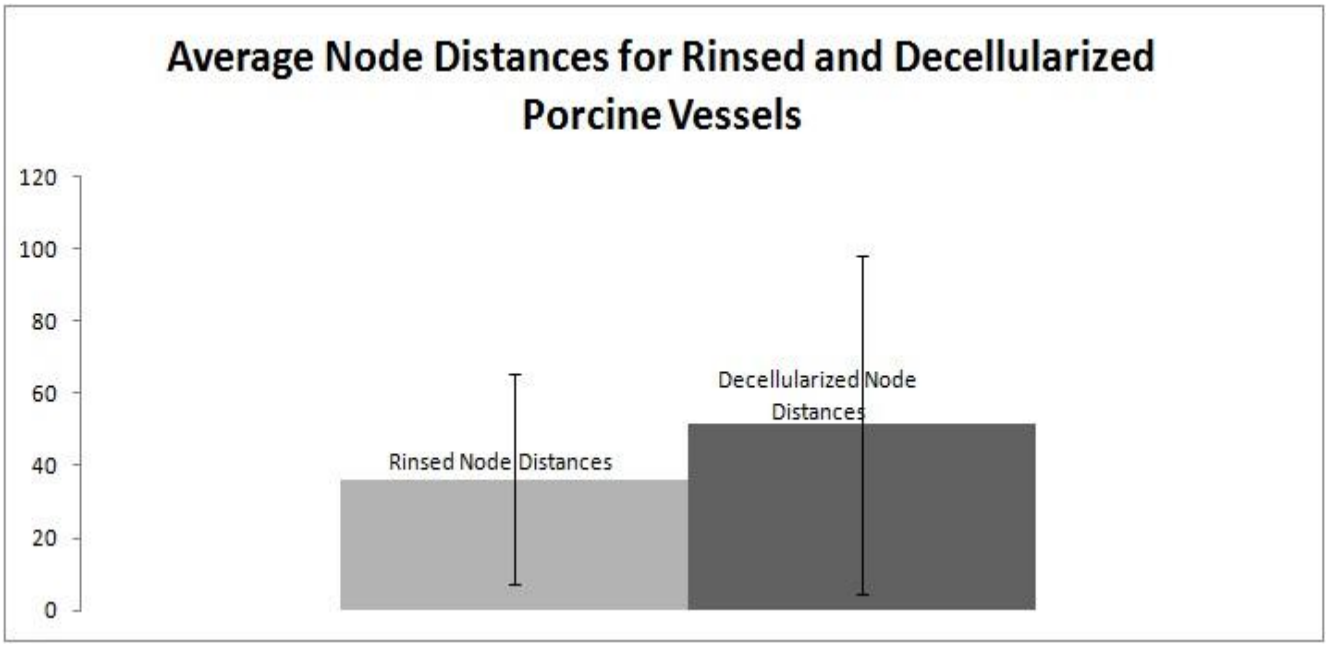

Figure 10. Graph of Node Distances. The average node distances of rinsed and decellularized vessels are shown.

The results from SEM analysis are tabulated in Table 1, Table 2, Table 3, and Table 4.

Table 1. Fiber Diameter Measurements of Rinsed Vessels at 500x using ImageJ.

Sample	Diameter 1	Diameter 2	Diameter 3	Diameter 4	Diameter 5	Average
3A	2.58	3.50	4.10	3.95	3.34	3.49
8A	4.56	3.50	7.60	5.78	4.86	5.26
3R	3.51	4.01	8.67	3.94	3.01	4.63
4R	4.80	7.38	6.74	6.52	4.59	6.01
5R	2.06	1.55	2.58	2.25	1.87	2.06
6R						
7R	3.80	3.32	3.53	5.02	4.34	4.00
8R	3.80	4.07	4.75	4.75	3.39	4.15

Table 2. Averages of Node Distances and Fiber Diameters for Rinsed and Decellularized Vessels at 500x using ImageJ.

Averages	Rinsed	Decellularized
Fiber Diameter (um)	3.49	3.06
Node Distance (um)	2.48	3.51

Table 3. Fiber Diameter Measurements of Decellularized Vessels at 500x using ImageJ.

Sample	Diameter 1	Diameter 2	Diameter 3	Diameter 4	Diameter 5	Average
2B	6.69	3.80	7.29	3.34	4.26	5.08
8B	6.84	3.95	4.56	4.56	5.62	5.11
3D	2.94	3.01	1.58	2.44	2.87	2.57
4D	2.22	1.93	1.58	1.93	1.50	1.83
5D	2.83	3.61	5.80	3.35	4.70	4.06
6D						
7D	3.39	3.39	4.54	4.61	3.32	3.85
8D	3.80	4.07	4.75	4.75	3.39	4.15

Table 4. Node Distance Measurements of All Vessels at 500x using ImageJ.

Sample	1	2	3	Average
3A	6	7	10	7.67
2B	26	31	18	25
8A	30	20	25	25
8B	16	22	24	20.67
3R	45	42	41	42.67
3D	75	117	193	128.3
4R	18	34	38	30
4D	127	68	135	110
5D	18	24	15	19
5R	16	27	19	20.67
6D				
6R				
7D	26	26	40	30.67
7R	35	13	44	30.67
8D	29	21	30	26.67
8R	77	86	130	97.67

3.2 Analysis of H&E Stained Images

Wide field microscopy produced images for qualitative results while Image-J analysis of the images provided quantitative results. There were three sets of samples from histology sectioning and staining that were imaged. The three sets were decellularized, rinsed, and control samples. Each set was imaged at magnifications of 4X, 10X, and 40X. 4X magnified images were used to determine the wall thickness. 10X and 40X magnified images were used to determine the presence of stained cells in the sample. Control samples were imaged; the magnified images of one are given in Figure 11. Figures 12 and 13 are the magnified images of the rinsed and decellularized vessels, respectively.

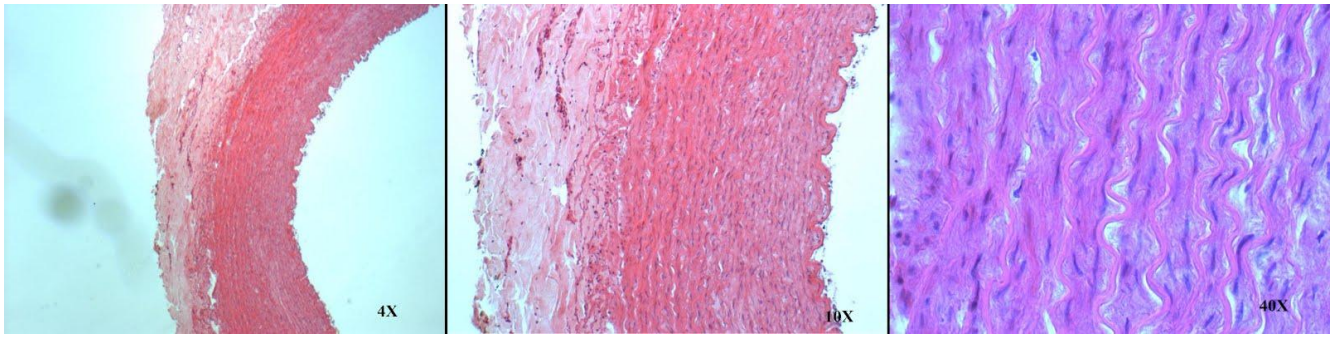

Figure 11. Control Vessel H&E. A cross section of a control vessel at 4X, 10X, and 40X magnification (left to right). Block 11-298.

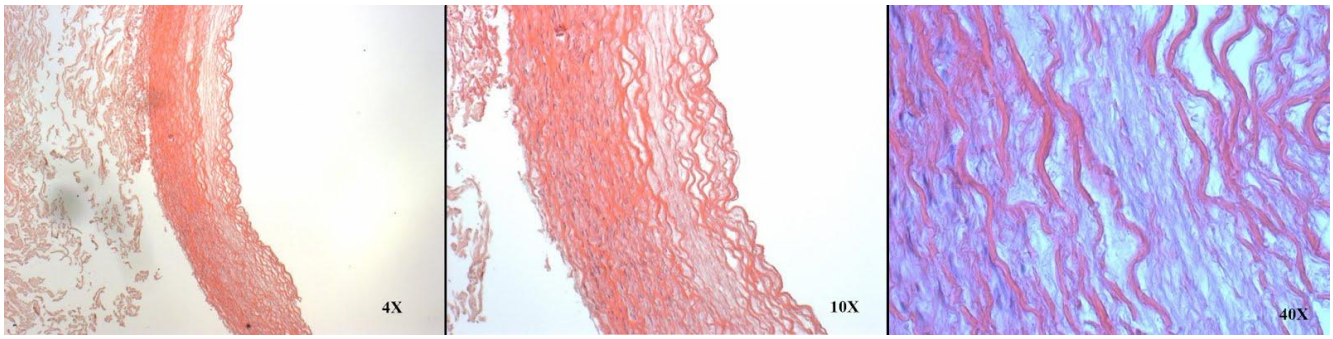

Figure 12. Rinsed Vessel H&E. The cross section of a rinsed vessel sample at 4X, 10X, and 40X magnification (left to right). Block 11-288.

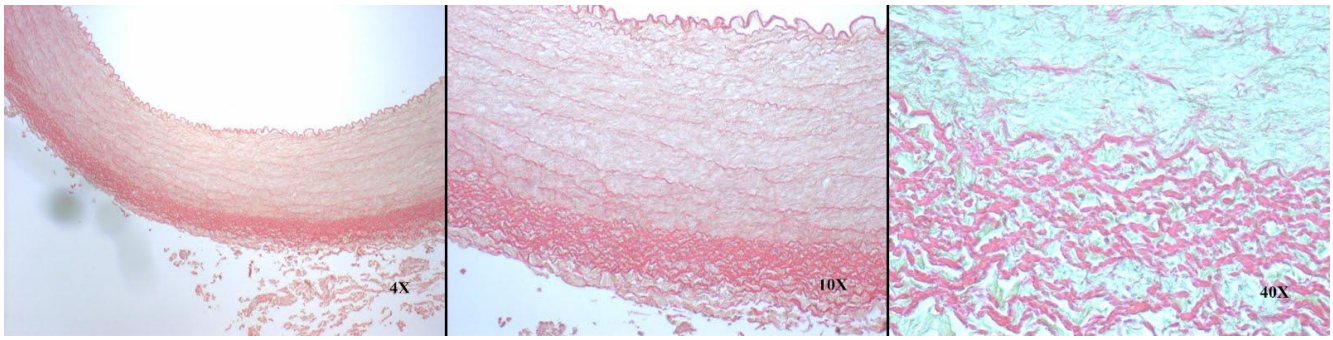

Figure 13. Decellularized Vessel H&E. A cross section of a decellularized vessel at 4X, 10X, and 40X magnification (left to right). Block 11-300.

The 10X and 40X magnifications of the control and rinsed vessels show the presence of cells by the dark blue stains (shown as dots). The images of the decellularized vessels show no presence of the cells which means that the decellularization process was successful.

The following tables are the tabulated results from analysis and measurement with Image-J along with cell presence. When measuring the wall thickness, the aventitia and any particulate tissues disconnected from the rest of the vessel were discounted from the wall thickness measurements. The image measurements of the control samples are listed in Table 5.

Table 6 lists all the measurements for the images of the rinsed vessel samples. Table 7 lists all the measurements for the images of the decellularized vessel samples.

Table 5. Control Sample Average Wall Thickness Measurements and Cell Presence.

Control		
Block	Cell Presence	Wall Thickness (mm)
11-298	yes	0.9615
11-325	yes	0.9744
11-348	yes	2.0353
11-349	yes	3.6819
11-350	yes	5.0377

Table 6. Rinsed Sample Average Wall Thickness Measurements and Cell Presence.

Rinsed		
Block	Cell Presence	Wall Thickness (mm)
11-278	yes	0.4311
11-279	yes	1.0769
11-280	yes	1.2492
11-281	yes	2.4383
11-282	yes	1.1587
11-283	yes	1.0633
11-284	yes	1.3886
11-285	yes	1.2540
11-326	yes	1.3093
11-328	yes	1.3742
11-339	yes	2.5537
11-341	yes	1.4511
11-344	yes	1.3133
11-347	yes	1.3349

Table 7. Decellularized Sample Average Wall Thickness Measurements and Cell Presence.

Decellularized		
Block	Cell Presence	Wall Thickness (mm)
11-300	no	1.1122
11-286	no	1.1466
11-287	no	1.0192
11-288	yes	0.8197
11-289	no	0.7997
11-290	no	1.2476
11-291	no	0.8333
11-292	no	0.9399
11-327	yes	0.8510
11-329	no	1.0457
11-338	no	1.5545
11-340	no	1.6210
11-345	no	1.2332
11-346	no	1.4912

The thickness values shown in the tables are all in the units of millimeters. The units were converted from pixels to millimeters by multiplying the measured thickness in pixels with the conversion factor, which was found to be 0.003205, to obtain the measurements in millimeters. The measurements in pixels were not included in the tables because pixels are not a common unit of measurement in this field. However, if ever needed, the measurements in units of pixels can be obtained by dividing the measurement in millimeters by the conversion factor.

The average wall thickness were put into graph form with standard deviation bars to effectively show the difference between rinsed and decellularized wall thickness in histological analysis. This graph is displayed in Figure 14.

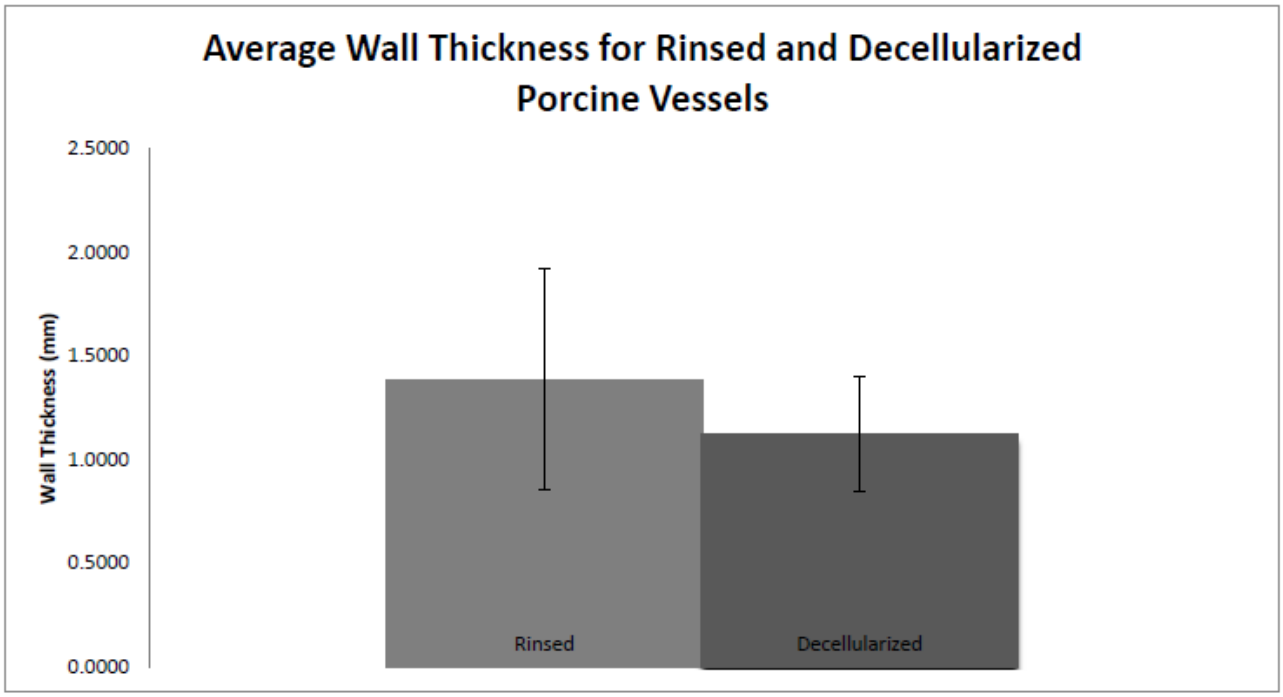

Figure 14. Graph of Average Wall Thickness. The average wall thickness of rinsed and decellularized vessels are shown.

3.3 Student T-Test Analysis

3.3.1 SEM

Figure 15 shows the results of the two-tailed t-test of two samples with unequal variances for the fiber diameters of the samples, excluding sample 6R and 6D. There was no significant difference observed as the p-value was 0.391, which is above the critical value of 0.05.

t-Test for Fiber Diameters: Two-Sample Assuming Unequal Variances

	Rinsed	*Decellularized*
Mean	3.629612714	4.228632143
Variance	1.561460464	1.612049685
Observations	7	7
Hypothesized Mean Difference	0	
df	12	
t Stat	-0.889651638	
P(T<=t) one-tail	0.195569768	
t Critical one-tail	1.782287548	
P(T<=t) two-tail	0.391139537	
t Critical two-tail	2.178812827	

Figure 15. Results of two-tailed t-test for fiber diameters. The results show no significant difference between the two samples.

Figure 16 shows the results of the two-tailed t-test of two samples with unequal variances for the node distances of the samples, excluding sample 6R and 6D. There was no significant difference observed as the p-value was 0.483, which is above the critical value of 0.05.

t-Test for Node Distance: Two-Sample Assuming Unequal Variances

	Rinsed	*Decellularized*
Mean	36.33571429	51.47714286
Variance	844.9825952	2180.750324
Observations	7	7
Hypothesized Mean Difference	0	
df	10	
t Stat	-0.728283678	
P(T<=t) one-tail	0.241572613	
t Critical one-tail	1.812461102	
P(T<=t) two-tail	0.483145226	
t Critical two-tail	2.228138842	

Figure 16. Results of two-tailed t-test for node distances. The results show no significant difference between the two samples.

3.3.2 H&E

Figure 17 shows the results of two-tailed t-test of two samples with unequal variances for the wall thickness of the samples. There was no significant difference observed as the p-value was 0.117, which is above the critical value of 0.05.

t-Test: Two-Sample Assuming Unequal Variances

	Rinsed	*Decellularized*
Mean	1.385473901	1.122481685
Variance	0.283717505	0.077136718
Observations	14	14
Hypothesized Mean Difference	0	
df	20	
t Stat	1.638102287	
P(T<=t) one-tail	0.058518956	
t Critical one-tail	1.724718218	
P(T<=t) two-tail	0.117037912	
t Critical two-tail	2.085963441	

Figure 17. Results of two-tailed t-test for wall thickness. The results show no significant difference between the two samples.

4. Discussion

The goal of Dr. Kristen Cardinal's laboratory research is to develop a successful BVM to be used for testing of intravascular devices. Intravascular device testing remains important for feasibility testing and regulatory purposes. Testing using BVMs could effectively reduce testing costs and time by increasing the understanding of the developing intravascular device before in-vivo testing.

This senior project, which is based off the research done by Professor Aubrey Smith, directly supports the research of Dr. Kristen Cardinal's lab. The goals of this senior project was to investigate decellularized blood vessels as a possible scaffold to use in a BVM. The characteristics of the vessels investigated in this project was wall thickness and fiber diameter which was studied using histology imaging and SEM imaging, respectively. The goal was to determine if the characteristics had statistically significant difference as a resulting from decellularization.

SEM imaging and analysis involved dehydrating the sample and imaging the vessel lumen in a scanning electron microscope. The fibers observed in the lumen were measured using Image-J and statistical analysis was done on the averages between rinsed and decellularized samples.

Histology imaging and analysis involved sectioning blocks obtained by embedding samples in paraffin wax. The slides were stained with H&E to stain for nuclei and the proteins in the ECM. Imaging was done using wide field microscopy. Analysis was done by looking for cell presence and measuring wall thicknesses in the sections. Statistical analysis was done on the average wall thicknesses between rinsed and decellularized samples.

From the SEM results, we observed trends of decreased fiber diameters and an increased node distances between rinsed and decellularized vessels. Intuitively, this is expected as the decellularization process removes cells and proteins, leaving behind only basement membrane. However, despite the slight changes, there were no significant differences between the two samples, indicating that the base architecture of the fibers remained the same between the two groups under SEM analysis. This reinforces other studies' results of an observed slight decrease in fiber diameter following decellularization but without statistical significance (23). Quantitatively, this shows no significant change in the physiologic characteristics of the lumen between rinsed and decellularized vessels. Qualitatively, this suggests that, while the fibers may be slightly weaker, there should not be a significant change in the tensile properties of the vessel following decellularization. Additionally, there were minimal breakage points observed in the decellularized vessels. To verify the strength of the vessels, future work may include tensile testing of both groups to compare relative Young's Moduli and ultimate tensile strengths.

Results from the H&E wide field microscopy demonstrated that the decellularization protocol was overall successful. Still, a few decellularized samples were found to have stained nuclei which could be attributed to the decellularization process. Another cause for this result, could be due to residual nuclei and nucleic acid remaining on the extracellular matrix. The quantitative analysis of H&E results showed trends of decreasing wall thickness. This same trend was seen in the SEM results. Again, the intuitive explanation of the removal of cells and proteins is attributed to the decrease in wall thickness. Proteins and cells are key to the structural integrity of the vessel and its removal from the vessel would cause changes to the overall structure. The changes happen to be a decrease in wall thickness and this was shown by averaging two differently treated samples. The rinsed vessesl, which maintained its structural integrity with

cells, were on average thicker than the decellularized vessels. In terms of developing a successful BVM, this could be a problem; however, the statistical analysis using a student t-test showed that the difference in wall thickness was not statistically significant. The results of this project showed a difference on average of wall thickness between rinsed and decellularized vessels with the given samples and sample size, but the difference was not significant enough for the vessels to be consistently different for the population. While, statistically, the difference was shown to be not significant, the difference was 19% loss in thickness due to decellularization. This is consistent with the work done by Sylvain Roy et al. where they found an average, between proximal and distal regions, of 44% thickness reduction after decellularization using their protocol. In their work, the samples that they used were untreated fresh samples and decellularized samples which could be attributed to the higher percentage seen in their study (24).

There are many roles of the wall thickness on the structural integrity as well as possibility to recellularize the scaffold. Wall thickness is an important factor in radial compliance for the vessel. A successful BVM should mimic the compliance of a untreated native vessel. The shown decrease in wall thickness may cause a change in compliance. Combining results from radial tensile testing to the wall thickness decrease could be used to correlate the decrease in wall thickness to compliance. This could be achieved statistically to determine if they are both related. Burst pressure can be affected by the wall thickness. Intuitively, a thinner wall thickness would correlate to a lower burst pressure. This can be shown by testing the decellularized vessels for burst pressure and comparing the values to those of rinsed vessels. The burst pressure could then be compared to the vessel wall thickness. This comparison could be done statistically to determine whether the burst pressure is a function of the vessel wall thickness.

Compliance and burst pressure could also be correlated to the fiber diameters. Fiber diameters have not been widely studied, but this project has shown that there is a small difference in fiber diameters between rinsed and decellularized vessel samples. The affect of this difference to compliance and burst pressure could be investigated by using the same statistical methods to be used for correlating wall thickness with compliance and burst pressure.

Limitations of this study lie in the processing of the porcine vessels. Porcine vessels were cut in half. One half were rinsed and the other half was decellularized. However, even though the samples came from the same vessel, the sections were large enough contain differences in wall thickness and surface morphology between the two sections. Vessels are not characteristically homogeneous throughout its length, so the differences could have affected the results. Another limitation of this study was in the preparation of the samples for imaging. In both SEM and histology for wide field microscopy, the samples were fixated and dehydrated before imaging. The fixation process may help proteins maintain it structure, but changes on the macroscopic scale may be significant. During SEM analysis, the dehydration process caused the vessel sample to shrink significantly. The results for fiber diameter shown in this project may not fully reflect the decellularization process, but rather the dehydration process. The same can be said for the histology analysis. Block preparation includes dehydration of the sample. The decellularization process may not have been fully reflected by the results for wall thickness.

Ultimately, the results do show a difference between rinsed and decellularized samples of porcine carotid arteries. This difference was not statistically significant as shown by the student t-test analysis. The results from this project support the possibility to use decellularized vessels as BVM for intravascular device testing. With the ability to effectively test intravascular devices ex-vivo, the cost of testing and time of testing could be significantly reduced. This could

effectively increase success rate of developing devices for regulation requirements and marketing. The lives of those who are affected by cardiovascular disease depend on the success of the developing devices. With improving intravascular devices, patients can receive better treatment.

5. References

1. World Health Organization. *Global Atlas on Cardiovascular Disease Prevention and Control*. Geneva: World Health Organization, 2011. Web. 02 Dec. 2011. <http://whqlibdoc.who.int/publications/2011/9789241564373_eng.pdf>.
2. "CDC - DHDSP - Heart Disease Facts." *Centers for Disease Control and Prevention*. Web. 02 Dec. 2011. <http://www.cdc.gov/heartdisease/facts.htm>
3. "Coronary Heart Disease - PubMed Health." Web. 02 Dec. 2011. <http://www.ncbi.nlm.nih.gov/pubmedhealth/PMH0004449/>.
4. "What Is Coronary Heart Disease? - NHLBI, NIH." *NIH Heart, Lung and Blood Institute*. Web. 02 Dec. 2011. <http://www.nhlbi.nih.gov/health/health-topics/topics/cad/>.
5. "ACE Inhibitors - Drug Class, Medical Uses, Medication Side Effects, and Drug Interactions by MedicineNet.com." Web. 02 Dec. 2011. <http://www.medicinenet.com/ace_inhibitors/article.htm>.
6. "Beta Blockers Drugs on MedicineNet.com." Web. 02 Dec. 2011. <http://www.medicinenet.com/beta_blockers/article.htm>.
7. "What Is a Stent? - NHLBI, NIH." *NIH Heart, Lung and Blood Institute*. Web. 02 Dec. 2011. <http://www.nhlbi.nih.gov/health/health-topics/topics/stents/>.
8. "Stent: MedlinePlus Medical Encyclopedia." *National Library of Medicine - National Institutes of Health*. Web. 02 Dec. 2011. <http://www.nlm.nih.gov/medlineplus/ency/article/002303.htm>.
9. Smith, Aubrey. “Characterization and Implementation of a Decellularized Porcine Vessel as a Biologic Scaffold for a Blood Vessel Mimic.” MS thesis California Polytechnic State University, 2011. Web.

10. Abbott WM, Mergerman J, Hasson JE, L'Italien G, Warnock DF. "Effect of compliance mismatch on vascular graft patency." *Journal of Vascular Surgery*. 5 (1987): 376-382.
11. Peter M. Crapo, Yadong Wang. "Physiologic compliance in small-diameter arterial constructs based on elastomeric substrate." *Biomaterials*. 31 (2010): 1626-1635.
12. A.P. Zhu, Zhang Ming, Shen Jian. "Blood compatibility of chitosan/heperin complex surfaces modified ePTFE vascular grafts." *Applied Surface Science*. 241 (2005): 485-492.
13. Nicolas L'Heureux, Stephanie Paquet, Raymond Labbe, Lucie Germain, Francois A. Auger. "A completely biological tissue-engineered blood vessel." *FASEB Journal*. 12 (1998): 47-56.
14. Swathi Ravi, Elliot L Chaikof. "Biomaterials for vascular tissue engineering." *Regenerative Medicine*. 5.1 (2010): 107.
15. Crispin Weinberg, Eugene Bell. "A Blood Vessel Model Constructed from Collagen and Cultured Vascular Cells." *Science*. 231(1986): 397-400.
16. Thomas W. Gilbert, Tiffany L. Sellaro, Stephen F. Badylak. "Decellularization of tissues and organs." *Biomaterials*. 27.19 (2006): 3675-3683.
17. K. Schenke-Layland, O. Vasilevski, F. Opitz, K. König, I. Riemann, K.J. Halbhuber, Th. Wahlers, U.A. Stock. "Impact of decellularization of xenogeneic tissue on extracellular matrix integrity for tissue engineering of heart valves." *Journal of Structural Biology*. 143.3 (2003): 201-208.
18. J.B.S. Conklin, E.R. Richter, K.L. Kreutziger, D.-S. Zhong, C. Chen. "Development and evaluation of a novel decellularized vascular xenograft." *Medical Engineering & Physics*. 24.3 (2002): 173-183.

19. Karnovsky, M.J. “A formaldehyde-glutaraldehyde fixative of high osmolality for use in electron microscopy.” *Journal of Cell Biology*. 27 (1965): 137-138.

20. *Preparation of Biological Samples*. University of Oklahoma. Web. 11 March 2012.

21. *Sample Preparation for Scanning Electron Microscopy – General Schedule for Animal Tissue*. University of Alabama. Web. 11 March 2012.

22. *U S Food and Drug Administration Home Page*. Digital image. *U S Food and Drug Administration Home Page*. Web. 1 Dec. 2011. <http://www.fda.gov/>.

23.Lu, Q. "Novel Porous Aortic Elastin and Collagen Scaffolds for Tissue Engineering. "*Biomaterials* 25.22 (2004): 5227-237. Print.

24.Roy, S. "Biomechanical Proprieties of Decellularized Porcine Common Carotid Arteries." *AJP: Heart and Circulatory Physiology* 289.4 (2005): H1567-1576. Print.

6. List of Appendices

Appendix A. *Dehydration Protocol*

1. Excise the sample from its given treatment
2. Place sample in the glutaraldehyde for at least 30 minutes
3. Rinse sample in distilled water 4 times
4. Place sample in 25% ethanol for 5 minutes
5. Place sample in 50% ethanol for 5 minutes
6. Place sample in 70% ethanol for 5 minutes
7. Place sample in 95% ethanol for 5 minutes
8. Place sample in 100% ethanol for 5 minutes
9. Let air dry
10. Mount the sample to a coverslip so that it is as flat as possible. Double stick tape can be used to adhere the sample to the coverslip
11. Image with the SEM

Appendix B. *Histology Preparation*

1. Fixation: Storage of samples within gluteraldehyde
2. Processing: Placement of samples within automated tissue processor to be immersed in increasing concentrations of alcohol, followed by a non-polar solvent such as xylene
3. Embedding: Samples are then placed into a metal mold which is then filled with molten paraffin wax. The samples are oriented so that the section of interest will be visible when the slices occur. The metal mold is then placed on a cold block to solidify the paraffin wax, effectively holding the sample in the orientation desired.
4. Sectioning: Paraffin blocks are secured in the microtome clamp and slowly moved closer to the spinning blade for slices of the sample to be taken. These slices are then mounted on to glass slides and covered using coverslips.
5. Staining: See Appendix C.
6. Microscopy: Stained samples will then be examined under a microscope. The samples will be analyzed to observe for any presence of nuclei within the decellularized sample.

Appendix C. *The staining protocol for an H&E stain (9).*

1. Place slides into the staining rack
2. Heat the staining rack in the oven for 5-10 min (the wax should be clear)
3. Pull the staining rack out of the oven and allow it to cool for 5 min
4. The slides are dipped in the following order for the given amount of time
    - 3 min - xylene (in the hood)
    - 3 min - xylene (in the hood)
    - 3 min - xylene (in the hood)
    - 2 min - 100% EtOH
    - 2 min - 100% EtOH
    - 2 min - 95% EtOH
    - 1 min - air dry
    - 4 min - hematoxlin
    - 1 min -distilled water
    - 30-45 sec - clearifier
    - 1 min - distilled water
    - 1 min - bluing
    - 1 min - distilled water
    - 1 min - 95% EtOH
    - 1 min 30 sec - Eosin
    - 1 min - 100% EtOH
    - 1 min - 100% EtOH
    - 1 min - 100% EtOH

- 3 min - Xylene (in the hood)
- 3 min - Xylene (in the hood)
- 3 min - Xylene (in the hood)

Appendix D. *University of Alabama, Sample Preparation (SEM) - Animal Tissue*

	Chemical	**Temperature**	**Time**	**Repetitions**
Primary Fixation	2.5% glutaraldehyde in distilled water	room or 0-4^{o}C	1-2 hours or microwave	1
Wash	Distilled water	room or 0-4^{o}C	10-20 minutes	3-5
Secondary Fixation	1-4% osmium tetroxide in distilled water	room or 0-4^{o}C	1-2 hours	1
Wash	Distilled water	room or 0-4^{o}C	10-20 minutes	3-5
Dehydration	25% ethanol 50% ethanol 70-75% ethanol 90-95% ethanol 100% ethanol	room or 0-4^{o}C	10 minutes 10 minutes 10 minutes 10 minutes 10 minutes	1 1 1 1 2
Critical Point Dry				
Mount on specimen stub with solver paste or graphite				
Coat with gold/palladium alloy				
Store stubs in desiccator				

Appendix E. *Measuring Lengths in Image-J*

1. Open up an image with Image-J. Image-J should open the chosen image in a new window.

2. When first opening up the program, the default units of measurement are pixels. The program needs the user to set a scale before outputting measurements in the units of micrometers.

3. To set a scale, first use Image-J's "Straight" tool to measure a known distance in the image.

    - Figure 18 is an image at 500x magnification that contains a scale of a known distance (200 micrometers) that can be measured.

    - To measure the scale, click the "Straight" button and then click and drag the line along the entire length of the scale. To finish measuring, go to "Analyze" in the tool bars and select "Measure" (or press CTRL+M).

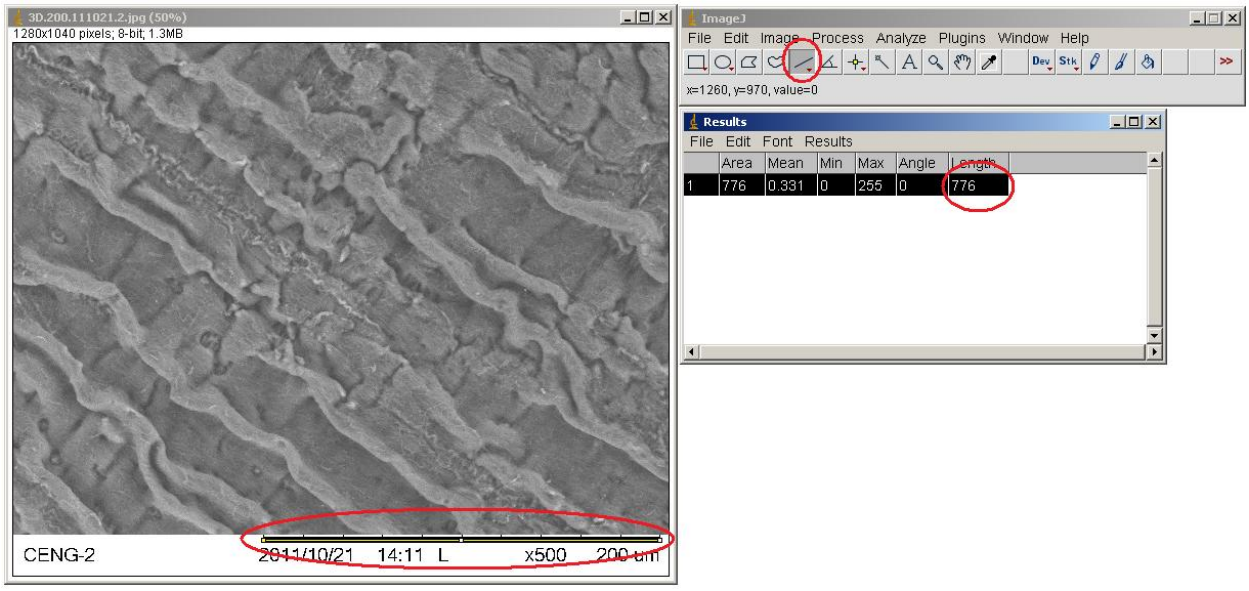

Figure 18. Image-J line measurement tool. The important parts described in this Appendix are circled in red.

4. The length of the measured scale should be given in pixels in the results box under the column "Length".

5. The scale length in pixels will be used to enter into the “Set Scale” option under “Analyze” in the toolbar. Figure 19 shows the set scale option.

- Enter the distance in pixels, known distance (200 um), pixel aspect ratio (which is 1 for a one to one ratio), and the units of the scale length (um). Confirm by pressing enter.

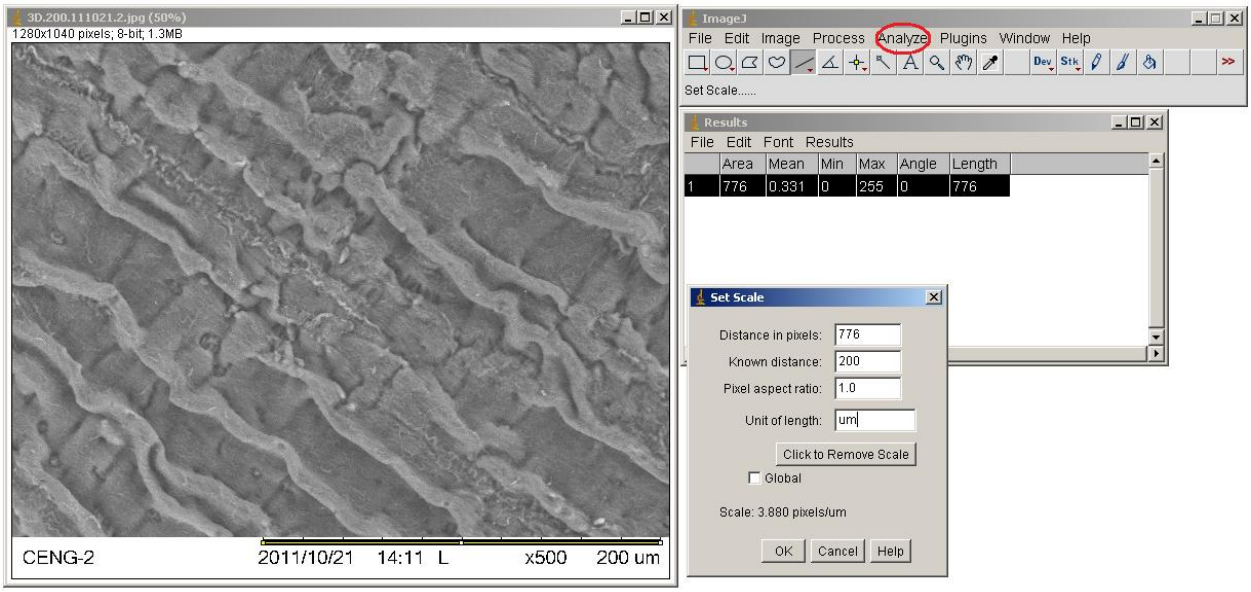

Figure 19. Set Scale option under the tab Analyze. Input the parameters in each box.

6. The scale has been set and all measurements taken after will output in micrometers. To double check, measure the known distance to see if the output is correct. (For this example, the output should be 200 micrometers.)